UCRL-52604

MEASURING THE PERMEABILITY OF ELEANA ARGILLITE FROM AREA 17, NEVADA TEST SITE, USING THE TRANSIENT METHOD

W. Lin

December 11, 1978

Work performed under the auspices of the U.S. Department of Energy by the UCLLL under contract number W-7405-ENG-48

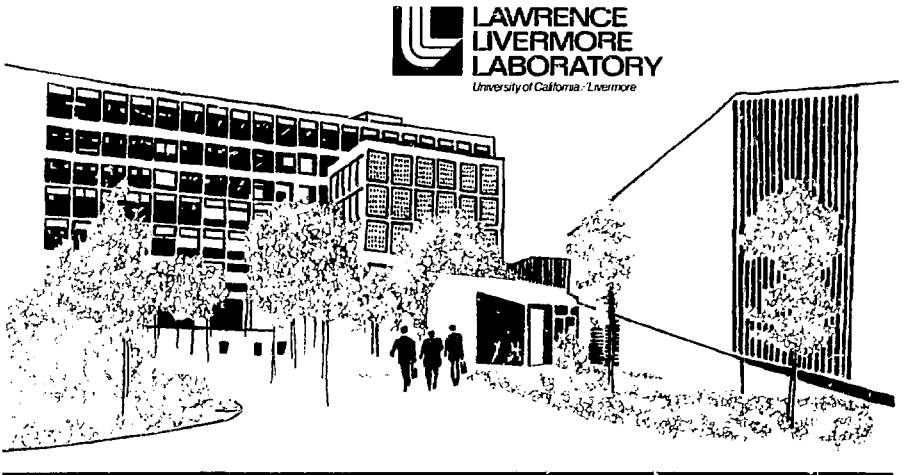

Distribution Category
UC-11,70

LAWRENCE LIVERMORE LABORATORY
University of California Livermore, California 94550

UCRL-52604

MEASURING THE PERMEABILITY OF ELEANA ARGILLITE FROM AREA 17, NEVADA TEST SITE, USING THE TRANSIENT METHOD

W. Lin

MS. date: December 11, 1978

CONTENTS

MEASURING THE PERMEABILITY OF ELEANA ARGILLITE FROM AREA 17, NEVADA TEST SITE, USING THE TRANSIENT METHOD

ABSTRACT

Using the transient method, we determine the permeability of high-quartz Eleana argillite from the Nevada Test Site as a function of effective pressure. By comparing calculated and observed pressure decay in the upstream reservoir, we have determined the permeability of intact and fractured specimens at effective pressures ranging from 1.0 to 24.0 MPa. Over this pressure range, Eleana argillite has a low permeability (10^{-16} to 10^{-19} cm^2) when intact and a higher permeability (10^{-12} to 10^{-17} cm^2) with one induced through-going fracture.

INTRODUCTION

When choosing a geological formation in which to permanently isolate nuclear wastes, one of our major concerns is transportation of radioactive materials to the biosphere by ground water. Therefore, the water permeability of *in situ* rock becomes a major criterion in the selection process. While the storage facility is being designed, it is necessary to have laboratory measurements of the water permeability of repository rocks as a function of stress, pressure, and temperature. During construction, while the repository is operating, and after it is closed, these data are needed for properly monitoring the repository's behavior.

The primary goal of the Terminal Waste Storage Program at the Nevada Test Site (NTS) is to evaluate the major geological formations with respect to suitability as locations for permanent storage of high-level radioactive wastes. NTS has a deep water table with long flow paths that eventually discharge into hydrologically closed basins, and there are a number of geological formations that might be suitable for radioactive waste storage. We examined one such site, an argillite (sometimes loosely termed "shale") in the Syncline Ridge block of the Eleana Formation.[1]

We measured the water permeability of intact and fractured specimens of high-quartz Eleana argillite as a function of effective pressure over a range of 1.0 to 24.0 MPa. Effective pressure is the confining pressure minus the pore pressure; we maintained the pore pressure at 50% of the confining pressure. This is a reasonable pore pressure to confining pressure ratio in a normal crustal condition.[2]

Although permeabilities from 10^{-13} to 10^{-7} cm^2 (10^{-5} to 10^{1} d) can be determined by steady-state methods, it is better to determine permeabilities less than 10^{-12} cm^2 by transient methods. Brace et al.[3] were the first to use the transient method to determine the permeability of Westerly granite as a function of pressure. Brace's simplified method works only if the pore volume is very small compared with the total volume of specimen and reservoir, and the bulk compressibility of rock is much smaller than the product of rock porosity and the compressibility of water. We used a more general approach,[4] the details of which are explained in the next section.

EXPERIMENTAL PROCEDURES

When the specimen (Fig. 1) is under a confining pressure, P_c, we saturate the specimen and bring it and the connected reservoirs to equilibrium at a pore pressure, P_p. Pore pressure is maintained at

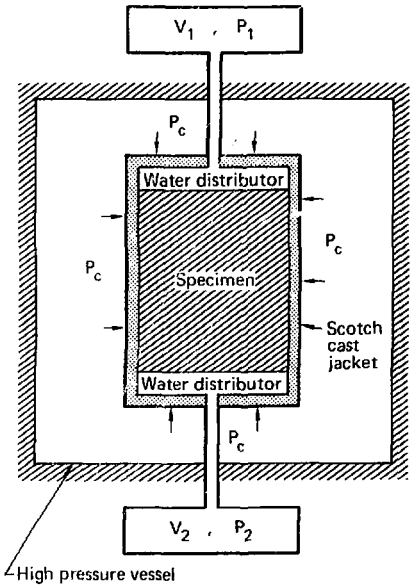

FIG. 1. Schematic diagram of the permeability measurement apparatus. V_1 and V_2 are the volumes of upstream and downstream reservoirs, respectively. P_1 and P_2 are the pressures in these reservoirs, P_c is the confining pressure.

half the confining pressure (Fig. 1). A small pressure increment, ΔP, is introduced in the upstream reservoir. The pressure decay in the upstream reservoir is then measured. Using a previously published model[4] that shows the relation between pressure decay and permeability, we determine the permeability of our specimens. Our specimens, apparatus, measurements, and calculations are explained in detail in the following subsections.

ROCK DESCRIPTION

The Eleana argillite cores are from the UE17$_c$ drill hole in the upper part of Unit J of the Eleana Formation, NTS, at Nevada State Coordinates N.260,057 (853,205) and E.197,037 (646,448). The hole, drilled by the U.S. Geological Survey, was 914.4 m deep. Our specimens are obtained from the massive, more or less uniform, argillite at depths greater than 73.5 m.

The argillite is entirely dark gray to black. Knife-blade penetration and electrical resistivity less than 20Ω-m indicate a clay content of from 50 to 90%.[1] The major minerals are quartz, illite, chlorite, kaolinite, pyrophyllite, and siderite. Quartz content affects the mechanical properties of the core: high-quartz argillite (x-ray studies show that the quartz content is 25–40%) is hard and strong after drying naturally. Low-quartz argillite (less than 25% quartz) dessicates and cracks when dry.[1] If water is added after drying, the rock becomes soft and falls apart.

Bedding planes are often obscure in the lower part of the argillite unit; dips range from 9 to 45° in the interval from 73.5 to 230 m. Dips are 30 to 80° at greater depths. The total porosity of argillite ranges from 6.8 to 13.5%.[1]

SPECIMEN PREPARATION

At the drill site, core material was carefully wrapped in aluminum foil and sealed with wax to prevent the loss—or gain—of water during storage. Cylindrical specimens, 2.54 cm in diameter and 3.81 cm long, were drilled from the drill-hole core, either parallel or perpendicular to the core axis. In the specimens that we studied, the bedding planes dip about 30 to 60° with respect to the specimen axis. The specimen ends were ground flat and parallel to each other, within 0.05 mm, across the diameter.

There were two types of specimen geometry. The first was an intact cylinder, with no visible faults or fractures. The second was identical to the first, except for one induced through-going fracture parallel to the specimen axis. We used the Brazil test (diametral loading along the cylindrical surface) to introduce a longitudinal, through-going, tensile fracture in specimens of the second geometry type. In all cases, prepared specimens were kept in a bell jar over water to prevent drying. All permeabilities were determined along the axial direction of the specimen.

Table I lists the specimens, their depths of origin, and their characteristics. We noticed that the specimens from deeper rock were denser and harder than the shallower ones. We tried to prepare the low-quartz argillite specimen by coring either with

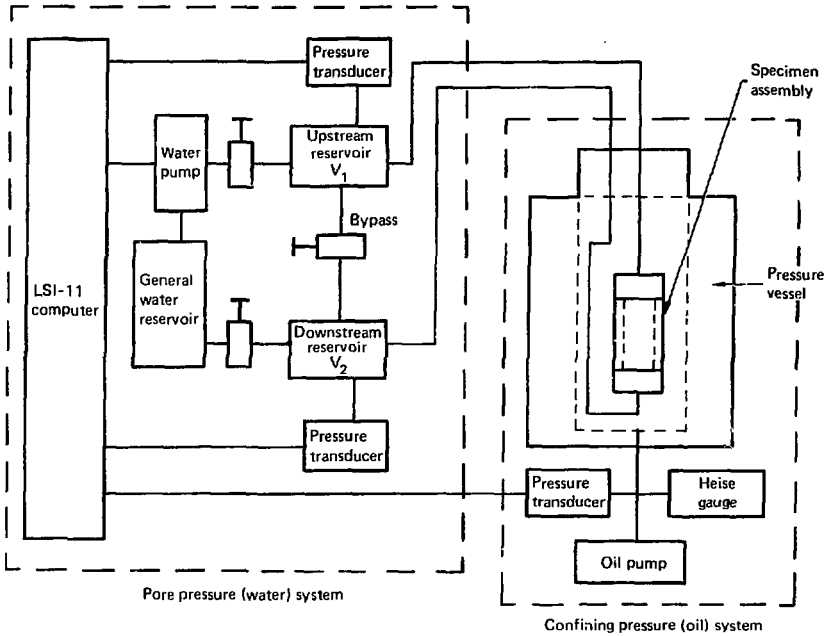

FIG. 2. Simplified diagram showing the connections among the three main parts of the permeability apparatus: specimen assembly, confining pressure system, and pore pressure system.

TABLE 1. Orientation, condition, and depth of origin of test specimens.[a]

Specimen No.	Depth, m	Test conditions	Orientation with respect to core axis
1	102.1	Intact	Parallel
2	102.1	Intact	Perpendicular
3	102.1	Fractured	Perpendicular
4	358.4	Intact	Perpendicular
5	358.4	Fractured	Perpendicular
6	361.2	Intact	Parallel
7	361.2	Fractured	Parallel

[a]Bedding planes of these specimens dip from 30 to 60° with respect to the specimen axis.

water or air, but the material is too weak for adequate preparation by either of these methods. All specimens in Table 1 are from the high-quartz group.

APPARATUS

The apparatus used in this study (Fig. 2) contains three main parts: the specimen assembly, the confining pressure system, and the pore pressure system. Heard and Duba have described the pore pressure system.[5]

The specimen assembly is held in a high-pressure vessel similar to those used in previous experiments.[6-8] Confining pressure is supplied by an air–oil hydraulic pump and monitored by a Heise gauge.

The two ends of the specimen assembly are connected to the upstream and downstream reservoirs (V_1 and V_2, respectively) by high-pressure capillary tubing. Water pressure in the reservoirs is supplied by an air–water hydraulic pump, which can be controlled manually or automatically, and measured by transducers. Reservoir pressure can be recorded manually or automatically by a LSI-11 microcomputer.

The specimen assembly, shown in detail in Fig. 3, is also similar to that used by Lakner.[6] The specimen is jacketed between two porous steel plates, which distribute water evenly over the specimen ends. The steel caps adjacent to the steel plates connect to the high pressure lines and the reservoirs. The entire unit is encased in Scotch Cast electrical resin 221, which prevents oil from penetrating the specimen. The casting resin is weak enough, however, to transmit hydrostatic pressure. Before casting, we clean the specimen surface and sand the surfaces of the steel end caps to ensure complete bonding of the Scotch Cast. The specimen assembly and high-pressure tubing are then connected to the high-pressure vessel plug.

MEASUREMENTS

Before measuring, we saturate the specimen with water and bring the pore pressure to half the desired confining pressure. Initially, confining pressure is the lithostatic pressure at the sample's original depth. To ensure that the specimen is fully saturated, we increase confining pressure step by step and keep the effective pressure as small as possible until the desired pore pressure is reached. During saturation, the bypass (Fig. 2) is open so that water can flow into the specimen from both ends. When the reservoir pressure does not vary more than the amount expected from thermal fluctuation for 24 hr, we assume that the specimen is saturated. After the reservoirs and specimen are equilibrated to the same pressure, we close the bypass and record the pressure change in each reservoir for one to two hours.

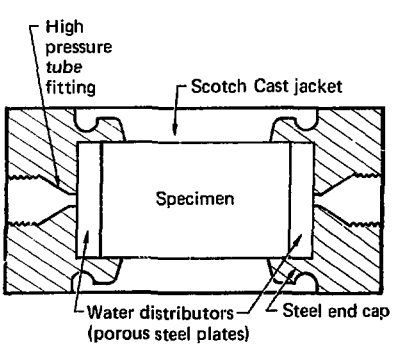

FIG. 3. The specimen assembly encases the specimen between porous steel plates, which act as water distributors.

After calibration, we increase the pressure in upstream reservoir (V_1) slightly and record the pressure variation as a function of time. This pressure increment, from 0.2 to 2.0 MPa, is usually much less than the pore pressure and does not noticeably affect the specimen permeability. Figure 4 shows one example of the observed pressure-time curve in the upstream reservoir after the pressure increment is introduced. The pressure has been normalized to a full scale of 2.0 MPa. Note that at the end of the run, the pressure increases with time; this is due to a slight increase in room temperature. The high-frequency fluctuation shown in Fig. 4 is the electrical noise from the system, particularly the pressure transducer.

With other parameters constant, the smaller the reservoir volume, the faster the pressure decays. Therefore, we used the pair of small reservoirs (5.95 and 9.25 cm^3) in all experiments with intact rock specimens of low permeability. The permeability of fractured specimens is high at low pressure; hence we used pairs of small (5.95 and 9.25 cm^3) and large (545 and 546 cm^3) reservoirs to double-check our measurements. At higher pressures, when the permeability of the fractured specimens is reduced, we use the small reservoirs. We believe that this method closely approximates the equivalent permeability of the fractured specimen. This is because the water flow through a fractured specimen may be quite different than the diffusion process we assumed in this study, especially at low pressure.

To correct pressure for the effects of leaks or temperature variation or both, we take the following steps: record the pressure variations as a function of time before and at the end of an experiment; fit straight lines to the pressure variation to obtain $\partial P/\partial t$ in the corresponding periods; take the mean of these two partial derivatives; and subtract—or

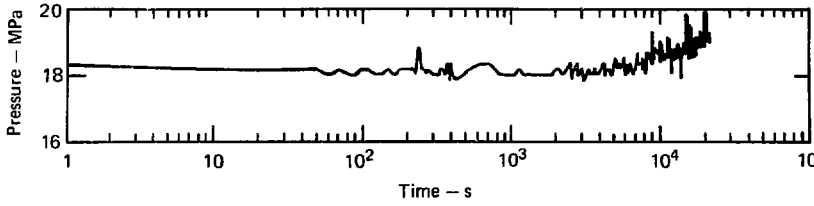

FIG. 4. Observed pressure variations as a function of time in the upstream reservoir. Specimen 1, with confining pressure = 2.8 MPa, pore pressure = 1.6 MPa, and pressure increment = 0.15 MPa. The pressure is normalized to 2.0-MPa maximum pressure.

add, depending on the sign of $\partial P/\partial t$—the mean $\partial P/\partial t$ from the observed pressure decay curve. We then compare the average of the observed curves (i.e., we disregard the electrical noise) with the calculated curves (next section, Fig. 5) to determine the specimen's permeability.

The data points in Fig. 5 are the corrected observed pressure variations in the upstream reservoir. This is the second run of specimen 1 (Table 1), at 2.8 MPa confining pressure and 1.6 MPa pore pressure. The permeability from this comparison is 1.5 to 2.0×10^{-17} cm^2.

MODEL STUDIES

As described above, we observe pressure decay over time in the laboratory. To obtain specimen permeability from the decay curve, we need to know the relation between specimen permeability and pressure decay in the reservoir. For a complete description of the model and the calculations, see Lin.[4] Briefly, the computer code TRUMP[9] is used to calculate one-dimensional fluid flow of water through a model system with the same dimensions as the real system, but with various permeability values. The input parameters—permeability, porosity, and compressibility of rock and viscosity and compressibility of water—are listed in Table 2; Fig. 6 is a sketch of the model configuration. In the calculations, the rock is divided into zones perpendicular to the direction of fluid flow; the number of zones is increased until the calculated results do not change significantly with further zonation.

Figure 5 shows the calculated pressure in the upstream reservoir as a function of time for a pair of reservoirs with volumes of 5.95 and 9.25 cm^3 and permeabilities from 10^{-19} to 10^{-12} cm^2. We compare these curves with the observed pressure-time curve to find the specimen's permeability.

EXPERIMENTAL UNCERTAINTIES

Two main sources account for the uncertainty of permeabilities determined by this method:

- Leaks and room temperature changes which effect pressure variation.
- Uncertainty about the true values of several parameters, particularly compressibility and viscosity of water, bulk compressibility, solid matrix compressibility, and the porosity of the specimen.

The effect of the first source is difficult to estimate. However, we believe that after the corrections shown in the last section, this factor makes our permeability in error by no more than 10%.

The compressibility and viscosity of water and the bulk compressibility of rock are the important factors in our second source of uncertainty. The porosity and the matrix compressibility of rock specimens, in this case, do not play important roles. A 5% decrease in the assumed compressibility of water (e.g., from 4.2 to 4.0×10^{-4} MPa^{-1}) will shift the calculated curve 15% toward the higher permeability end. However, the compressibility of water is quite independent of pressure in the pressure range of interest.[10] We do not expect the compressibility of water to deviate more than 2% from the value we used; its effect on error is therefore no more than 4%. A 10% increase in bulk compressibility of this rock (e.g., from 1.4 to 1.54×10^{-4} MPa^{-1}) shifts the calculated curves by 10% toward the higher permeability end. We believe that the average static bulk compressibility

TABLE 2. Input parameters to model studies.

Parameter	Value	Remarks
Upstream reservoir volume (V_1), cm^3	5.94 and 546	Fig. 2, actual size as that used in experiment
Downstream reservoir volume (V_2), cm^3	9.25 and 545	"
Sample cross-section area (A), cm^2	5.07	"
Sample length (L), cm	3.81	"
Compressibility of water (β), MPa^{-1}	4.2×10^{-4}	Kennedy and Holser, Ref. 10
Bulk compressibility of shale (β_{eff}), MPa^{-1}	1.4×10^{-4}	Averaged static bulk compressibility of Eleana argillite from depths up to 367m at 0.1MPa. (H.+M. Laboratory, Mercury, Nevada, 1977, unpublished data.)
Compressibility of solid matrix of shale (β_s), MPa^{-1}	2.66×10^{-5}	Compressibility of Devonian shale at 1.0 GPa (Lin, unpublished data, 1978)
Viscosity of water (μ), Pa-s	1.0×10^{-3}	Viscosity of water at 20°C and 0.15 to 100.0 MPa (Clark, Ref. 12)
Porosity of shale (ϕ)	0.05	0.5 of the averaged porosity of Eleana shale (argillite) (Hudson and Hoover, Ref. 1)[a]
Permeability (κ), cm^2	10^{-19} to 10^{-12}	Range of expected permeability

[a]We arbitrarily assume that the connected porosity of Eleana argillite is 0.5 of its total porosity. It is shown that in this case, the porosity does not affect the calculated pressure decay significantly.

of Eleana argillite from depths up to 367 m (Table 2) does not differ from that of Eleana argillite specimens we used by more than 10%; the bulk compressibility of rock introduces an error of no more than 10%, therefore. The probable error of viscosity is 1 to 2%; the corresponding error in permeability is about the same. Varying the rock porosity from 0.05 to 0.1 or from 0.05 to 0.01 contributes to the error of permeability no more than 1 to 2%. When we sum all these potential error factors, we estimate that the uncertainty of the permeability values is within 20% of the values reported in Table 3.

RESULTS AND DISCUSSION

Typical results from our argillite specimens are shown in Fig. 7 and summarized in Table 3. Figure 7 shows the permeabilities of specimens 6 and 7 (see Table 1 for their descriptions) as a function of effective pressure. These two specimens were taken from the same sample block; the effect of an induced fracture can be seen. In both specimens, the permeability, κ, decreases with increasing effective pressure, P_e.

In Fig. 8, the data from Fig. 7 are replotted in a log κ vs log P_e scale. Clearly, permeability varies with negative power of effective pressure, i.e., $\kappa \propto P_e^N$. Other specimens, except for 1 and 2, show the same characteristics.

The same negative power relation holds in specimens 1 and 2 if we disregard the data at the effective pressure of 24.1 MPa. The possible decrease in bulk compressibility of rock at higher pressure

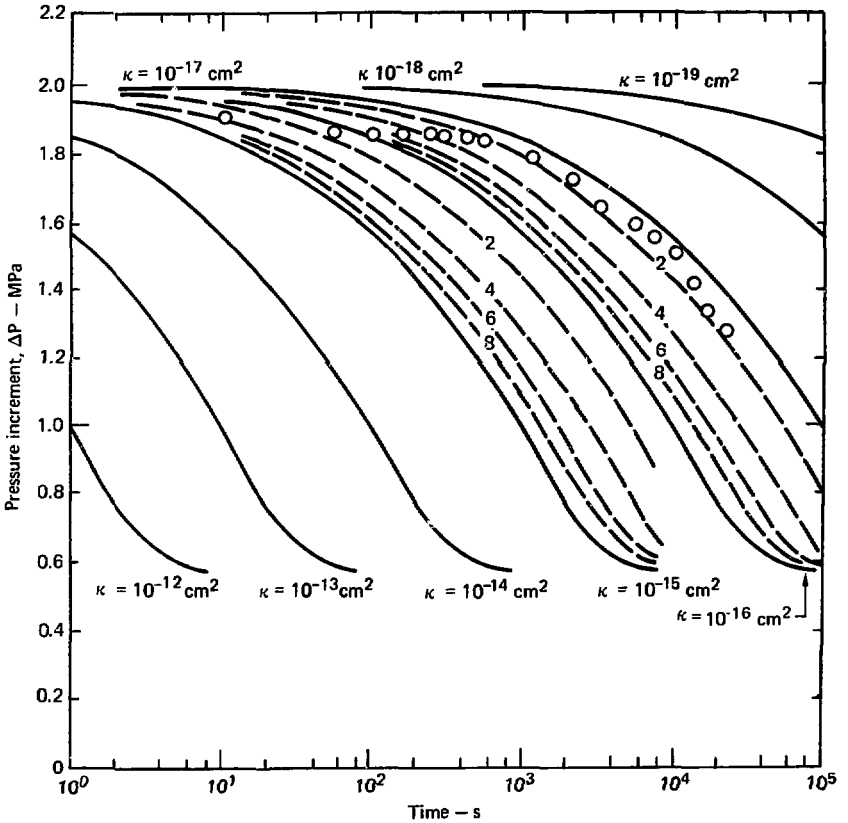

FIG. 5. Comparison of corrected observation (O) with calculated pressure decay curves (solid and dashed lines) for specimen 1. Permeability (κ) is determined to be 1.5 to 2.0 $\times$ 10^{-17} cm ^{2}.

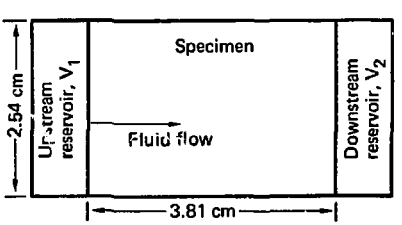

FIG. 6. Configuration of model study. V_1 and V_2 are the volumes of the upstream and downstream reservoirs, respectively; fluid flows from V_1 to V_2.

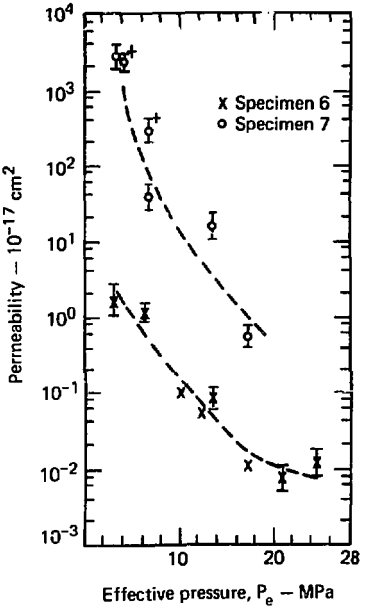

FIG. 7. Permeability of Eleana argillite as a function of effective pressure for specimens 6 (intact) and 7 (fractured) from 361.2 m deep. The dashed lines are drawn to show the trend of the data. † data are the data from large-reservoir experiments.

may make the determined permeability too small. Although this may not fully explain the low permeability of these two specimens at 24.1 MPa effective pressure, we consider that the negative power is a good approximation for the data of these two specimens.

We calculated N values by the least-squares method, as shown in Table 3. We can see from Table 3 that a fractured specimen has an N value much greater than that of the corresponding intact specimen. This is because closing a fracture is much easier than closing pores. Generally, intact argillite specimens have permeabilities at the lower end of

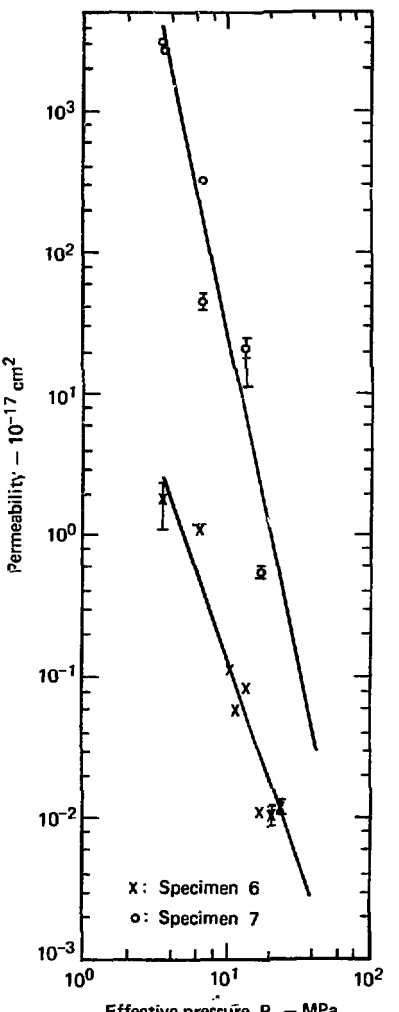

FIG. 8. Log-log plot of permeability of specimens 6 and 7 as a function of effective pressure. The straight lines are fitted by the least-squares method.

TABLE 3. Permeability of Eleana argillite as a function of pressure and effective pressure.

Specimen No.	Depth, m	Condition, orientation[a]	Confining pressure, MPa	Effective pressure (P_e), MPa	Permeability (κ), 10^{-17} cm^2	N ($\kappa \propto P_e^N$)
1	102.1	Intact,	2.8	1.1	3.2 ~ 3.7	−0.28[b]
		parallel	2.8	1.2	1.5 ~ 2.0	±0.09
			20.7	10.1	1.2	
			48.3	24.1	0.3	
			27.6	13.1	1.1	
			2.8	1.2	2.2	
2	102.1	Intact,	2.8	1.3	5.5	−0.6[b]
		perpendicular	2.8	1.3	8.0 ~ 10.0	±0.17
			6.9	3.5	6.1 ~ 8.1	
			20.7	10.0	1.2 ~ 2.2	
			34.5	16.8	2.2	
			48.3	24.1	$(1.2 \sim 3.0) \times 10^{-1}$	
			27.6	13.7	1.1	
3	102.1	Fractured,	2.8	1.2	$8.5 \times 10^4 \sim 1.1 \times 10^5$[c]	−3.6
		perpendicular	6.9	3.3	$6.1 \times 10^4 \sim 1.1 \times 10^5$[c]	±0.59
			20.7	10.3	$(2.2 \sim 6.1) \times 10^1$	
			48.3	24.0	3.2 ~ 5.0	
			48.3	23.7	8.1 ~ 11.0	
4	358.4	Intact,	6.9	3.2	0.8 ~ 1.1	−2.0
		perpendicular	48.3	24.0	$(1.1 \sim 2.2) \times 10^{-2}$	
5	358.4	Fractured,	6.9	3.4	$8.1 \times 10^2 \sim 1.1 \times 10^3$	−5.7
		perpendicular	6.9	3.3	$(2.2 \sim 3.7) \times 10^3$[c]	±0.94
			13.8	6.8	11.0 ~ 22.0	
			13.8	6.1	22.0 ~ 35.0	
			20.7	9.5	2.2 ~ 4.2	
			34.5	16.9	1.1 ~ 2.0	
			48.3	23.4	0.6 ~ 1.0	
6	361.2	Intact,	7.0	3.5	1.1 ~ 2.4	−3.0
		parallel	13.8	6.3	1.1 ~ 1.2	±0.34
			20.7	10.3	1.1×10^{-1}	
			27.6	13.3	$(8.1 \sim 9.0) \times 10^{-2}$	
			27.6	12.1	6.0×10^{-2}	
			34.5	17.0	1.1×10^{-2}	
			41.4	20.7	$9.1 \times 10^{-3} \sim 1.2 \times 10^{-2}$	
			48.3	24.1	$(1.1 \sim 1.3) \times 10^{-2}$	
7	361.2	Fractured,	7.0	3.4	$(2.4 \sim 4.0) \times 10^3$	−4.7
		parallel	7.0	3.5	$(2.4 \sim 3.0) \times 10^3$[c]	±0.75
			13.8	6.6	$(2.4 \sim 4.0) \times 10^2$[c]	
			13.8	6.6	$(4.0 \sim 5.0) \times 10^1$	
			27.6	13.3	$(1.1 \sim 2.5) \times 10^1$	
			34.5	17.1	$(5.0 \sim 6.0) \times 10^{-1}$	

[a]Condition is either intact or fractured. Orientation is either parallel or perpendicular to core axis.
[b]Data at 24.1-MPa effective pressure are not used to calculate N.
[c]Data are obtained by using pair of large reservoirs (546 and 545 cm^3).

the range (4×10^{-4} to 10^{-17} cm^2) of shale[13]; these permeabilities are two to three orders of magnitude lower than the permeabilities published for Westerly granite[2] and Barre granite.[14]

As shown in Fig. 7, a single through-going fracture in the specimen increases its permeability significantly. The lower the effective pressure, the more pronounced the permeability increase. Table 3 shows that this holds for all the specimens we studied. Table 3 and Fig. 7 also show that, at low pressure, the permeability of a fractured specimen is about four orders of magnitude greater than that of the corresponding intact specimen; at higher pressures, the difference is one to two orders of magnitude. This permeability difference is probably due to permanent damage to the fractured surface during the fracture process. Also, because of the bedding of the specimen, the induced fracture is neither straight nor smooth. The fracture surface may not completely close up at high pressure. It is possible that there are scale effects of fractured permeability versus *in situ* fracture permeability. We do not take it into consideration in this laboratory study. The scale effect can be evaluated when the effect of fracture interaction on permeability is determined.

Our results indicate that the permeability of Eleana argillite is virtually constant along the axial and radial directions of the core axis (specimens 1 and 2, 4 and 6, 5 and 7). As mentioned in the rock description, the bedding planes of these specimens dip from 30 to 60° to the specimen axis. The isotropic character of permeability with respect to the bore-hole axis may be an effect of bedding dip rather than an intrinsic property of the rock. To study the effect of bedding plane on permeability, we would have to test specimens either parallel or perpendicular to the bedding.

Our results also show that the depth of origin of the specimen may affect permeability. This is true for both intact and fractured specimens. The intact specimens from 102.1 m deep (specimens 1 and 2) have a permeability about one to two orders of magnitude greater than that of intact specimens from 358.4 and 361.2 m deep (specimens 4 and 6). This difference is more pronounced at high pressure than at low pressure.

We have not attempted to study the time dependence of permeability. When we removed specimens from the apparatus at the ends of the experiments, we did observe that water left in the steel cap was contaminated by clay mineral particles. This may be due to the disturbance of the specimen during handling. It is not likely that mineral particles have been transported from the specimen. However, the importance of dissolving clay minerals in water on permeability variation over long periods is not yet clear.

Kranz et al.[14] reported that with effective pressure kept constant, the permeability of jointed Barre granite decreased with increasing P_p/P_c ratio. We have not attempted to study this effect on the Eleana argillite. As mentioned in the Introduction, 0.5 is a reasonable P_p/P_c ratio in a normal crustal condition.

CONCLUSIONS

From the viewpoint of water transport at room temperature, high-quartz Eleana argillite seems a viable alternate for repositories for highly radioactive waste for either Westerly or Barre granite. Within the argillite itself, the permeability seems to decrease with increasing depth. We were not able to prepare the low-quartz specimen for permeability measurement. The effect of low-quartz content on the permeability of Eleana argillite must be further studied. The effects of temperature, time, and anisotropy on permeability must also be thoroughly investigated.

Although one induced through-going fracture increases the permeability significantly, the increase is not prohibitively great at high pressure. For a reasonably deep repository (500 to 2000 m deep), the presence of the fractures themselves would not necessarily exclude storing nuclear wastes safely. A more exact analysis, relating the effect of fracture interaction to permeability, is needed.

ACKNOWLEDGMENTS

D. Trimmer was indispensable for maintaining the permeability apparatus. We thank R. L. Kranz for making a preprint of his paper available. Discussion with H. C. Heard was helpful. The author thanks L. D. Ramspott, D. L. Hoover, and W. Ellis for their helpful comments.

REFERENCES

1. J. N. Hudson and D. L. Hoover, *Geology of the UE17e Drill Hole, Area 17, NTS*, U.S. Geological Survey Rept., in press.
2. M. K. Hubbert and W. W. Rubey, "Mechanics of fluid-filled porous solids and its application to overthrust faulting," *Geol. Soc. Am. Bull.*, **70**, 115 (1959).
3. W. F. Brace, J. B. Walsh, and W. T. Frangos, "Permeability of Granite Under High Pressure," *J. Geophys. Res.* **73**, 2225 (1968).
4. W. Lin, *Compressible Fluid Flow Through Rocks of Variable Permeability*, Lawrence Livermore Laboratory, Livermore, Calif., UCRL-52304 (1977).
5. H. C. Heard and A. G. Duba, *Capabilities for Measuring Physicochemical Properties at High Pressure*, Lawrence Livermore Laboratory, Livermore, Calif., UCRL-52420 (1978).
6. J. F. Lakner, *A New Apparatus for Permeability Measurements Under Litho-Static Conditions and Results on Drop Fractured and High Explosive Fractured Oil Shale*, Lawrence Livermore Laboratory, Livermore, Calif., UCRL-50562 (1968).
7. R. Quong and V. J. La Guardia, *Permeability of Pictured Cliffs Sandstone: Gasbuggy Preshot and Postshot Measurements*, Lawrence Livermore Laboratory, Livermore, Calif., UCRL-50946 (1970).
8. R. Quong and J. Baker, *Computer-Controlled Apparatus for Permeability Measurements at Confining Pressures up to 10^2 Pascal (10^3 bar)*, Lawrence Livermore Laboratory, Livermore, Calif., UCID-30073 (1974).
9. A. L. Edwards, *TRUMP: A Computer Program for Transient and Steady-State Temperature Distributions in Multidimensional Systems*, Lawrence Livermore Laboratory, Livermore, Calif., UCRL-14754, Rev. 3 (1972).
10. G. C. Kennedy and W. T. Holser, "Pressure-Volume-Temperature and Phase Relations of Water and Carbon Dioxide," in *Handbook of Physical Constants*, S. P. Clark, Jr., Ed. (Geological Society of America, Memoir 97, 1966), p. 371.
11. F. Birch, "Compressibility: Elastic Constants," in *Handbook of Physical Constants*, S. P. Clark, Jr., Ed. (Geological Society of America, Memoir 97, 1966), p. 167.
12. S. P. Clark, Jr., "Viscosity of Water and Steam," in *Handbook of Physical Constants*, S. P. Clark, Jr., Ed. (Geological Society of America, Memoir 97, 1966), p. 300.
13. M. Gondouin and C. Scala, "Streaming Potential and the SP Log," *J. Petrol. Tech.* **10** (AIME Tech. Paper 8023), 170 (1958).
14. R. L. Kranz, A. D. Frankel, T. E. Engelder, and C. H. Schalz, *The Permeability of Whole and Jointed Barre Granite* (submitted to *Int. J. Rock Mech. Min. Sci*) . . .

BSS